Journal of Earthquake Engineering
Publication details, including instructions for authors and subscription information:
http://www.tandfonline.com/loi/ueqe20

A Probabilistic Methodology to Determine Elastic Acceleration Response Spectra for Pulse-Type Records through Multi-Resolution Analyses

Long-jun Xu[a], Guo-Chen Zhao[a], Ya-bin Chen[a] & Li-li Xie[a]
[a] Department of Civil Engineering, Harbin Institute of Technology at Weihai, Weihai, China
Published online: 28 Jul 2015.

Journal of Earthquake Engineering, 00:1–27, 2015

ISSN: 1363-2469 print / 1559-808X online
DOI: 10.1080/13632469.2015.1045104

Taylor & Francis
Taylor & Francis Group

A Probabilistic Methodology to Determine Elastic Acceleration Response Spectra for Pulse-Type Records through Multi-Resolution Analyses

LONG-JUN XU, GUO-CHEN ZHAO, YA-BIN CHEN, and LI-LI XIE

Department of Civil Engineering, Harbin Institute of Technology at Weihai, Weihai, China

This article focuses on the characterizations of pulse-type ground motions which are mainly caused by rupture directivity. Multi-resolution analysis is employed to decompose 53 typical pulse-type records which are selected from 12 large earthquakes into a series of ground motion components. A methodology for deriving design spectra, which could incorporate the special effects caused by pulse-type records is proposed based on the bi-normalized response spectra of ground motion components, and is named as Near-Fault Response Spectrum (NFRS). Analysis results indicate that NFRS might be a reliable candidate for the code-based design spectrum especially for structures constructed close to active fault.

Keywords Pulse-type Ground Motions; Acceleration Response Spectrum; Bi-Normalized Response Spectrum; Multi-Resolution Analysis; Seismic Design

1. Introduction

Pulse-type ground motions, which are generally particular to the forward direction, where the fault rupture propagates towards the site at a velocity close to shear wave velocity, have caused much of the damage in recent major earthquakes [Somerville *et al*., 1997; Hall *et al*., 1995]. This type motion is characterized by a large amplitude and long period velocity pulse that exposes the structure to high input energy at the beginning of the record, and has been identified as imposing extreme demands on structures to an extent. [Adanur *et al*., 2012; Ghahari *et al*., 2010; Galal and Ghobarah, 2006]. Many scholars have pointed out that the seismic design of a building which constructed close to an active fault should account for these special aspects of pulse-type ground motions [Hall *et al*., 1995; Somerville *et al*., 1997; Alavi and Krawinkler, 2000]. The near-source factors recommended presently may be considered as a stopgap measure that gives recognition to the problem but does not necessarily provided a final answer. Analyses indicated that this method cannot solve the problem consistently, because design procedures should pay attention to the special frequency characteristics of pulse-type ground motions [Alavi and Krawinkler, 2000]. The analyses performed in Somerville [2003] indicated that the shape of the intermediate- and long-period part of the response spectrum of pulse-type motions changes as the level of the spectrum increases and as the magnitude increases, such that this type motions cannot be adequately described by a fixed response spectral shape. In addition, the pulse-type records

Received 17 December 2014; accepted 19 April 2015.

Address correspondence to Guo-Chen Zhao, Department of Civil Engineering, Harbin Institute of Technology at Weihai, Weihai 264209, China. E-mail: zgc011@126.com

Color versions of one or more of the figures in the article can be found online at www.tandfonline.com/ueqe.

show a large diversity, which has hindered incorporating this special effect of pulse-type records by traditional method such as response spectra [Akkar *et al*., 2005; Baker, 2007; Luco and Cornell, 2007]. Hence, additional work in the area of earthquake engineering and civil engineering is warranted.

The majority of earthquake design spectra are obtained by averaging a set of response spectra from records with similar characteristics such as soil condition, epicentral distance, magnitude, source mechanism, etc. [Hubbard and Mavroeidis, 2011]. To practical applications, smoothing is carried out to eliminate the peaks and valleys in the response spectra. Peak ground motion (peak ground acceleration, velocity, and displacement), duration of strong motion, and frequency content are the three important parameters for ground motions in earthquake engineering applications. In previous analyses, response spectra were usually normalized with the peak ground motion or other similar parameters such as spectrum intensity, effective peak acceleration, etc., so the influence of peak ground motion on response spectra can be eliminated to an extent. Previous research work has shown that strong motion duration may largely influence the inelastic demand of short-period structures with stiffness and strength degradation [Bommer *et al*., 1999, 2004; Hancock and Bommer., 2007; Montejo and Kowalsky, 2008]. But for elastic systems, the effects caused by duration of strong motion are inconspicuous. Therefore, frequency content is the last and the most critical factors that influence the characterizations of response spectra. The analyses performed in Pavel *et al.* [2014] indicated that the frequency content is responsible for the large variations of the spectral values and for the spectral shape.

Fourier amplitude spectrum and power spectral density are the two commonly used methods to characterize the frequency content of ground motions in frequency domain. The frequency domain characterization of a ground motion only implies a stochastic process having a relatively uniform distribution of energy throughout the duration of the motion, so a time-domain representation would be more preferable [Bray and Rodriguez-Marek, 2004]. In addition, these methods can only characterize the frequency content of ground motions, but it cannot eliminate the influence of frequency content on response spectra. For eliminating the influence caused by frequency contents on response spectra, a period and/or a frequency parameter is used to normalize the abscissa axis of response spectrum. This method has been widely used in seismic response analysis, and Xu and Xie [2004] first termed the response spectrum obtained by this method as bi-normalized response spectrum. Xu and Xie [2004] used strong ground motions recorded during the 1999 Chi-Chi earthquake to obtain bi-normalized spectra for four soil types. The same authors Xu and Xie [2007] developed bi-normalized pseudo velocity response spectra by using a database of 53 near-fault ground motions. Ziotopoulou and Gazetas [2010] and Gazetas [2012] compared the dynamic amplification factor obtained from normalized spectra with that obtained from bi-normalized spectra, and concluded that the current code value of 2.5 underestimates the real ratio S_a/PGA, especially in the region close to the predominant period of the ground motions, where the actual value approaches 3.75. Maniatakis and Spyrakos [2012] proposed a new methodology to determine elastic displacement spectra which is expressed in a standard and in a bi-normalized form. Pavel *et al.* [2014] investigated the bi-normalized response spectra for recorded strong ground motions with various frequency contents and pointed out that the bi-normalized dynamic amplification factor response spectrum might be a reliable candidate for the code-based design spectrum. But, in the case of strong motions, such as pulse-type motions, with multiple peaks or with no predominant peak, the definition of the predominant period is rather vague [Maniatakis and Spyrakos, 2012]. As a result, bi-normalized response spectrum has not yet been adopted by current seismic design codes, mostly because of the ambiguity regarding the determination of the dominant period.

In this article, an approach for deriving acceleration spectra which could incorporate the special aspects of pulse-type records is proposed and investigated. This methodology is mainly based on the bi-normalized response spectra of ground motion components instead of original records, which is different from traditional methods. Probabilistic methods for evaluating the acceleration amplitudes of ground motion components are introduced. For obtaining reliable ground motions components, multi-resolution analysis, one of the main contents in wavelet analyses, is employed in this study. Five kinds of ground motion components are then defined which are used to investigate the influence of frequency content on response spectra. 53 pulse-type ground motions which are assembled by Bray and Rodriguez-Marek [2004] are utilized in this study. At last, the proposed spectrum is compared with the design spectra of Chinese code (GB50011-2010), European code (Eurocode 8) and American code (UBC97, IBC 2012). Key insights from this study are then summarized, and the content needed to be further studied is discussed.

2. Multi-Resolution Decomposed Method

A complicated function can be divided into several simpler ones through wavelet analyses and then study them separately [Ruch and Van Fleet, 2009]. A major reason for the popularity of wavelets is their efficiency in the representation of non-stationary signals, such as ground motions. It can be conducive to represent the signal as a summation of wavelets rather than a summation of stationary harmonic waves [Ruch and Van Fleet, 2009]. Multi-resolution analysis, one of the main contents of wavelet analyses, can compactly represent signals in several levels of resolutions [Mallat, 1989] and is introduced to decompose pulse-type ground motions in this study. There is a wide literature available regarding theoretical features of the approach as well as algorithmic details, so only a brief overview of the most relevant features is provided here.

Let V_j, $j \in \mathbf{Z}$, be a sequence of subspaces of $L^2(\mathbf{R})$. $\{V_j\}_{j\in\mathbf{Z}}$ is a multi-resolution analysis of $L^2(\mathbf{R})$ if

$$V_j \subset V_{j-1} \qquad \text{(nested)}$$

$$\overline{\bigcup_{j\in\mathbf{Z}} V_j} = L^2(\mathbf{R}) \qquad \text{(density)}$$

$$\bigcap_{j\in\mathbf{Z}} V_j = \{0\} \qquad \text{(separation)}$$

$$f(t) \in V_{j-1} \Leftrightarrow f(2t) \in V_j \qquad \text{(scaling)}$$

There exists a scaling function $\phi(t)$, such that the set $\{\phi_{j,k}(t) = 2^{-j/2}\phi(2^{-j}t - k),\ k \in \mathbf{Z}\}$ is a orthonormal basis for V_j. In V_j arbitrary function can be expressed the linear combination of $\{\phi_{j,k}(t)|k \in \mathbf{Z}\}$. So in V_j the approximation of the target function $x(t)$ is:

$$x^j(t) = \sum_k < x(t),\ \phi_{j,k}(t) > \phi_{j,k}(t) \qquad (1)$$

It is necessary to obtain the details (or error) as the target function is moved from one approximate space to the next. W_j is wavelet space. There exists a wavelet function

$\psi(t)$, such that the set $\{\psi_{j,k}(t) = 2^{-j/2}\psi(2^{-j}t - k),\ \ k \in \mathbf{Z}\}$ is an orthonormal basis for W_j. If $x^j(t)$ and $x^{j-1}(t)$ are projections of $x(t)$ in V_j and V_{j-1} respectively, the residual function $w^j(t) = x^j(t) - x^{j-1}(t)$ is the orthogonal projection of $x(t)$ into W_j. So $w^j(t)$ can be expressed as:

$$w^j(t) = \sum_k < x(t),\ \psi_{j,k}(t) > \ \psi_{j,k}(t) \tag{2}$$

W_j is the orthogonal complement of V_j in V_{j-1}. Hence, $L^2(\mathbf{R})$ can be written as:

$$L^2(\mathbf{R}) = W_1 \oplus W_2 \oplus W_3 \oplus \cdots \oplus V_j. \tag{3}$$

The space partition is illustrated in Fig. 1. So any $x(t) \in L^2(\mathbf{R})$ can be written as:

$$x(t) = \sum_{i=1}^{j} w^i(t) + x^j(t) \tag{4}$$

Besides, there is a straightforward process to recover $x^j(t) \in V_j$ from the projection of $x^{j+1}(t)$ into V_{j+1} and $w^{j+1}(t)$ into W_{j+1}. Mallat algorithm (Eqs. (5)–(7)) is used to conduct the decomposition and reconstruction of pulse-type motions. Set $x(t)$ is a given pulse-type records. And the length is n. $x^j(t)$ is the projections of $x(t)$ in V_j, and the length is $n/2^j$. x_k^j is the kth number in $x^j(t)$. And $w^j(t)$ and w_k^j can be defined as the same way. $x^{j+1}(t)$, $w^{j+1}(t)$ and $x^j(t)$ can be calculated by Eqs. (5)–(7), where h_{n-2k} and g_{n-2k} is weight coefficient:

$$x_k^{j+1} = \sum_n h_{n-2k} x_n^j \tag{5}$$

$$w_k^{j+1} = \sum_n g_{n-2k} x_n^j \tag{6}$$

$$x_n^j = (\sum_k h_{n-2k} x_k^{j+1} + \sum_k g_{n-2k} w_k^{j+1}) \tag{7}$$

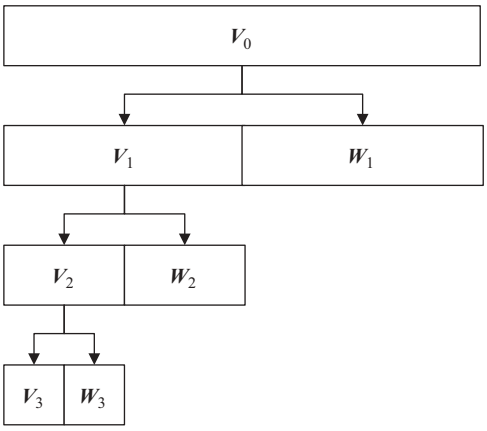

FIGURE 1 Space partition for multi-resolution analysis.

Apparently, if the reconstruction is performed by Eq. (7) completely, the original record will be obtained again. For obtaining a series of components with different frequencies, single refactoring is performed based on the wavelet coefficients obtained in the process of decomposition. In this study, w^1, w^2, . . . , w^j, x^j are solely reconstructed from $\boldsymbol{V}_1$, $\boldsymbol{V}_2$, . . . , $\boldsymbol{V}_j$ to space $\boldsymbol{V}_0$ and denoted as w_1, w_2, . . . , w_j, x_j, respectively. So a given ground motion $x(t)$ can be represented by components in several levels of resolutions:

$$x(t) = w_1 + w_2 + \cdots + w_j + x_j \tag{8}$$

For better understanding, w_1, w_2, . . . , w_j, x_j are denoted as C_1, C_2, . . . , C_j, C_{j+1}, where "C" is the abbreviation of "Component." It is clear that determining the maximum resolution "j" is the key factor in the process of decomposition. In this study, if w_{j+1} and/or x_{j+1} do not present obvious oscillation characteristics and/or their acceleration amplitudes are lower than the 1% of the acceleration amplitude of the corresponding original record, then "j" is defined as the maximum resolution.

Acceleration and velocity time histories of an original ground motion (OGM) recorded of the TCU103 station during Chi-Chi earthquake and those of its 7 components are shown in Figs. 2 and 3, respectively. The period T_i $i = 1, 2, 3, 4, 5, 6, 7$ shown in Figs. 2–3 is the predominant period which associated with the peak value of the absolute acceleration response spectrum for corresponding ground motion component. As shown in Figs. 2–3, the vibration frequency of each component is close to a constant, but different from each other.

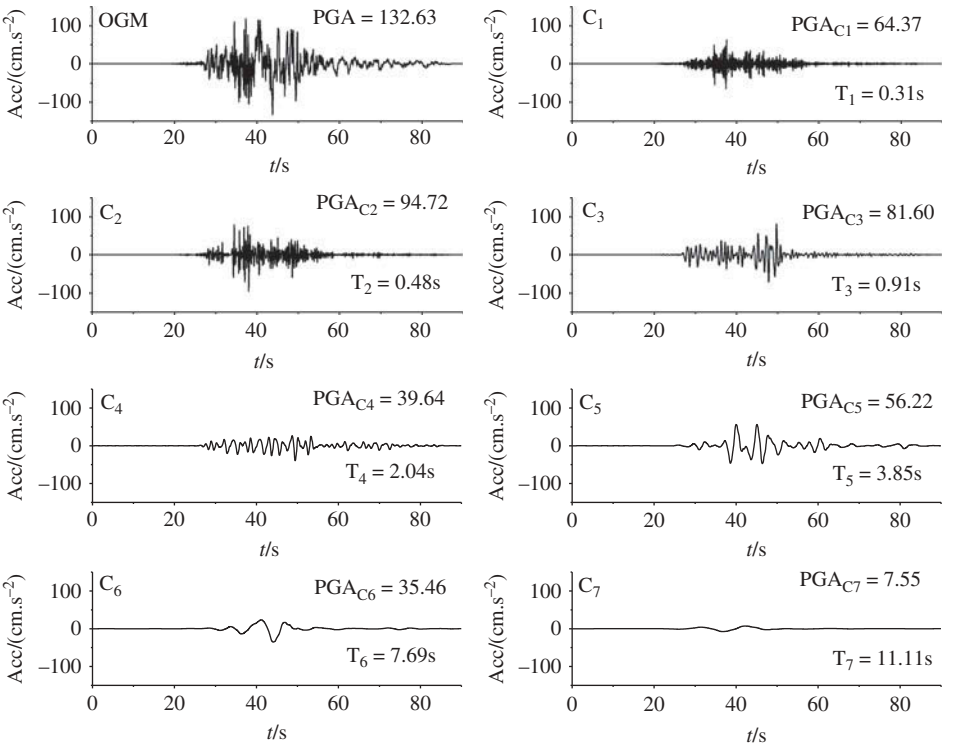

FIGURE 2 Acceleration time-histories of the ground motion that recorded of TCU103 station during Chi-Chi earthquake and those of its seven ground motion components.

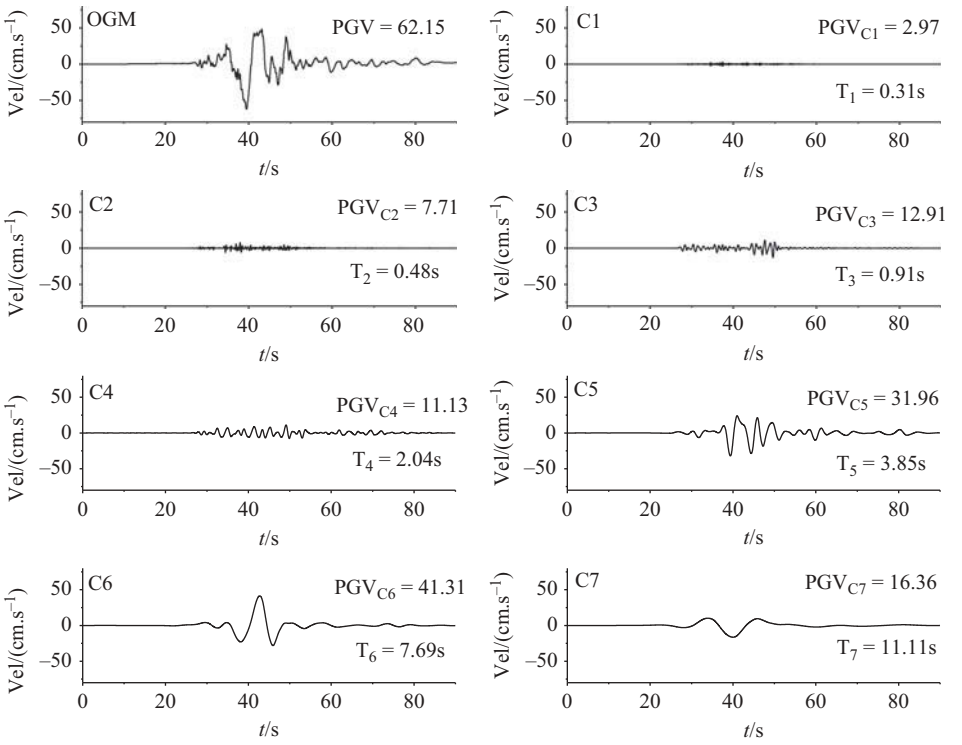

FIGURE 3 Velocity time-histories of the ground motion that recorded of TCU103 station during Chi-Chi earthquake and those of its seven ground motion components.

3. Recordings Utilized in This Study and Definitions of Several Kinds of Ground Motion Components

3.1. Pulse-Type Ground Motion Records

Sets of recorded pulse-type ground motions assembled by Bray and Rodriguez-Marek [2004] are utilized in this study. All of these records are typical forward-directivity ground motions, and are selected from the strong motion database of the Pacific Earthquake Engineering Research Center (http://peer.berkeley.edu/). These records are restricted to those from shallow earthquakes in active tectonic regions. Table 1 lists the relevant information of these selected ground motions. More detailed information of these records and the criteria for their incorporation into the forward-directivity ground motion database is given in Bray and Rodriguez-Marek [2004]. The distribution of the ground motion sites with magnitude and distance is shown in Fig. 4.

3.2. Definitions of Several Kinds of Ground Motion Components

After the decomposition of the 53 pulse-type records through multi-resolution decomposed method, 466 components are obtained. Analyses preformed in frequency domain indicate that the frequency contents of these components are visibly simple than those of original records, because of the very narrow-band distribution of these components in frequency domain. These components are named as simple component (SC) in this article.

TABLE 1 Stations included in the analysis of near-fault ground motions (compiled by Bray and Rodriguez-Marek, 2004)

No.	Earthquake	Station	Distance R(km)	Site	PGA /g	PGV /(cm.s^{-1})	PGD /cm
1	Parkfield	Cholame#2	0.1	Soil	0.47	75	22.5
2	(1966/06/27,	Temblor	9.9	Rock	0.29	17.5	3.17
	$M_w = 6.1$)						
3	San Fernando	Pacoima dam	2.8	Rock	1.47	114	29.6
	(1971/02/09,						
	$M_w = 6.6$)						
4	Imperial Valley	Brawley airport	8.5	Soil	0.21	36.1	14.6
5	(1979/10/15,	EC County center FF	7.6	Soil	0.22	54.5	38.4
6	$M_w = 6.5$)	EC Meloland overpass FF	0.38	Soil	0.38	115	40.2
7		EI Centro arrar#10	8.6	Soil	0.23	46.9	31.4
8		EI Centro arrar#3	9.3	Soil	0.27	45.4	17.9
9		EI Centro arrar#4	4.2	Soil	0.47	77.8	20.7
10		EI Centro arrar#5	1	Soil	0.53	91.5	61.9
11		EI Centro arrar#6	1	Soil	0.44	112	66.5
12		EI Centro arrar#7	10.6	Soil	0.46	109	45.5
13		EI Centro arrar#8	3.8	Soil	0.59	51.9	30.8
14		EI Centro diff. Array	5.3	Soil	0.44	59.6	38.7
15		Holtville post office	7.5	Soil	0.26	55.1	33
16		Westmorland fire sta	15.1	Soil	0.1	26.7	19.2
17	Morgan Hill	Coyote lake dam	0.1	Rock	1	68.7	14.1
18	(1984/04/24,	Gilroy array#6	11.8	Rock	0.61	36.5	6.6
	$M_w = 6.2$)						
19	Superstition Hills	EI Centro Imp. co. cent	13.9	Soil	0.31	51.9	22.2
20	(1987/11/24,	Parachute test site	0.7	Soil	0.42	107	50.9
	$M_w = 6.6$)						
21	Loma Prieta	Gilroy-gavilan coll.	11.6	Rock	0.41	30.8	6.5
22	(1989/10/17,	Gilroy-historic bldg.	12.7	Soil	0.29	36.8	10.1
23	$M_w = 7.0$)	Gilroy array#1	11.2	Rock	0.44	38.6	7.2
24		Gilroy array#2	12.7	Soil	0.41	45.6	12.5
25		Gilroy array#3	14.4	Soil	0.53	49.3	11
26		LGPC	6.1	Rock	0.65	102	37.2
27		Saratoga-Aloha Ave	13	Soil	0.38	55.5	29.4
28		Saratoga-W Valley Coll.	13.7	Soil	0.4	71.3	20.1
29	Erzican, Turkey	Erzincan	2	Soil	0.49	95.5	32.1
	(1992/03/13,						
	$M_w = 6.7$)						
30	Northridge	Jensen filter plant	6.2	Soil	0.62	104	45.2
31	(1994/01/17,	LA dam	2.6	Rock	0.58	77	20.1
32	$M_w = 6.7$)	Newhall-fire Sta	7.1	Soil	0.72	120	35.1
33		Newhall-W. Pico Cyn. Rd	7.1	Soil	0.43	87.7	55.1
34		Pacoima dam (downstr)	8	Rock	0.48	49.9	6.3
35		Pacoima dam (upper left)	8	Rock	1.47	107	23

(*Continued*)

TABLE 1 (Continued)

No.	Earthquake	Station	Distance R(km)	Site	PGA /g	PGV /(cm.s^{-1})	PGD /cm
36		Rinaldi receiving Sta	7.1	Soil	0.89	173	31.1
37		Sylmar-converter Sta	6.2	Soil	0.8	130	54
38		Sylmar-converter Sta E	6.1	Soil	0.84	116	39.4
39		Sylmar-olive view FF	6.4	Soil	0.73	123	31.8
40	Kobe, Japan	KJMA (Kobe)	0.6	Rock	0.85	96	24.5
41	(1995/01/17,	Kobe University	0.2	Rock	0.32	42.2	13.1
42	$M_w = 6.9$)	OSAJ	8.5	Soil	0.08	19.9	9.2
43		Port Island (0 m)	2.5	Soil	0.38	84.3	45.1
44	Kocaeli, Turkey	Arcelik	17	Rock	0.21	42.3	44.4
45	(1999/08/17,	Duzce	12.7	Soil	0.37	52.5	16.4
46	$M_w = 7.4$)	Gebze	17	Rock	0.26	40.7	39.5
47	Chi-Chi, Taiwan	TCU052	0.2	Soil	0.35	159	105.1
48	(1999/09/21,	TCU068	1.1	Soil	0.57	295.9	101.4
49	$M_w = 7.6$)	TCU075	1.5	Soil	0.33	88.3	39.5
50		TCU101	2.9	Soil	0.2	67.9	75.4
51		TCU102	1.8	Soil	0.3	112.4	89.2
52		TCU103	4	Soil	0.13	61.9	87.6
53	Duzce, Turkey (1999/11/12, $M_w = 7.1$)	Bolu	17.6	Soil	0.82	62.1	13.6

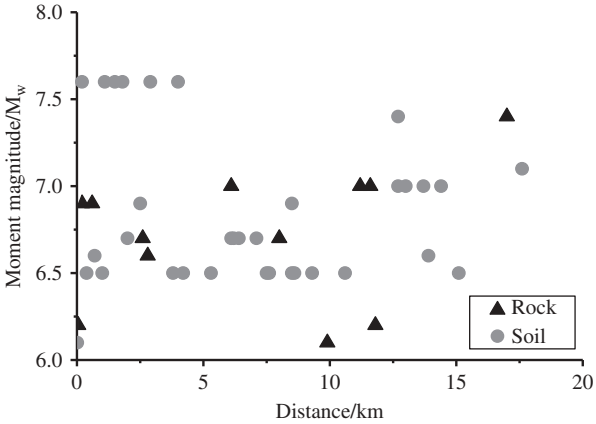

FIGURE 4 Distribution of pulse-type recordings utilized in this study.

Two combination components, low-frequency component (LFC) and high-frequency component (HFC), are defined. LFC is the linear superposition of SC with period larger than 1 s, and HFC is the linear superposition of SC with period less than 1 s. It should be noted that there are no specific meanings of defining 1 s as the cut-off period. Actually, there is no clear definition for what long-period is and what short-period is. Investigating

the influence of frequency content on response spectrum is the main purpose of analyzing combination components. So precisely defining the cut-off period is not very important.

The major feature for pulse-type ground motion differing from others will be the large velocity pulse. Much effort has been devoted to the representation of the large velocity pulse through simplified pulse model [Makris, 1997; Krawinkler and Alavi, 1998; Menum and Fu, 2002; Mavroeidis *et al*., 2003] and/or decomposed method, such as moving average filtering [Ghahari *et al*., 2010] and wavelet analyses [Baker, 2007; Yaghmaei-Sabegh, 2010, 2012]. As mentioned above, a series of simple components can be obtained by multi-resolution decomposed method. Analyses indicate that the simple component with the largest velocity amplitude can represent the major feature of the corresponding original pulse both in frequency and time domain. The component with the largest velocity amplitude is used as a simplification of original velocity pulse, and is named as predominant component (PC). The detailed information of predominant component is given in Zhao and Xu [2013]. The residual component (RC) which does not include the large velocity pulse is investigated in this study as well.

As shown in Figs. 2 and 3, C_1–C_7 are simple component; the summation of C_1–C_3 is the high-frequency component; the summation of C_4–C_7 is the low-frequency component; C_6 is the predominant component, and OGM - C_6 is the residual component.

4. Statistical Characterizations of Response Spectra

4.1. Statistical Characterizations of Normalized Response Spectra

Undoubtedly, the peak ground acceleration of original record PGA_O shows a large diversity for different original records, and the peak ground acceleration of ground motion component PGA_C shows a large diversity for different ground motion components. In this study, the acceleration response spectrum of original ground motion is normalized by PGA_O, and the acceleration response spectrum of ground motion component is normalized both by PGA_O and PGA_C, respectively. Figure 5 shows the statistical parameters (mean value, variance, and coefficient of variation, which are given in Eqs. (9)–(11), respectively) of the normalized response spectra for original ground motions and ground motion components, and all of the ordinates are normalized by PGA_O:

$$E[X|_{T=t}] = \sum_{i=1}^{53} x_i|_{T=t} /53 \tag{9}$$

$$\sigma^2 = [\sum_{i=1}^{53} (x_i|_{T=t} - E[X|_{T=t}])^2]/53 \tag{10}$$

$$C.V|_{T=t} = \sigma|_{T=t} /E[X|_{T=t}] \tag{11}$$

Figure 5a indicates that: (1) the spectral acceleration of OGM is mainly dominated by LFC and HFC in long- and short-period region, respectively; (2) a number of non ignorable low-frequency components are still included in RC, in consideration of the large spectral acceleration of RC in long-period region; and (3) PC cannot represent the spectral characterizations of original record in long-period region, in consideration of its small spectral values. Figure 5b shows the variance of the normalized response spectra for these five sets of data. It can be seen that the variance of OGM is mainly dominated by LFC and HFC in long- and short-period region, respectively, which behaves the same trend with the mean

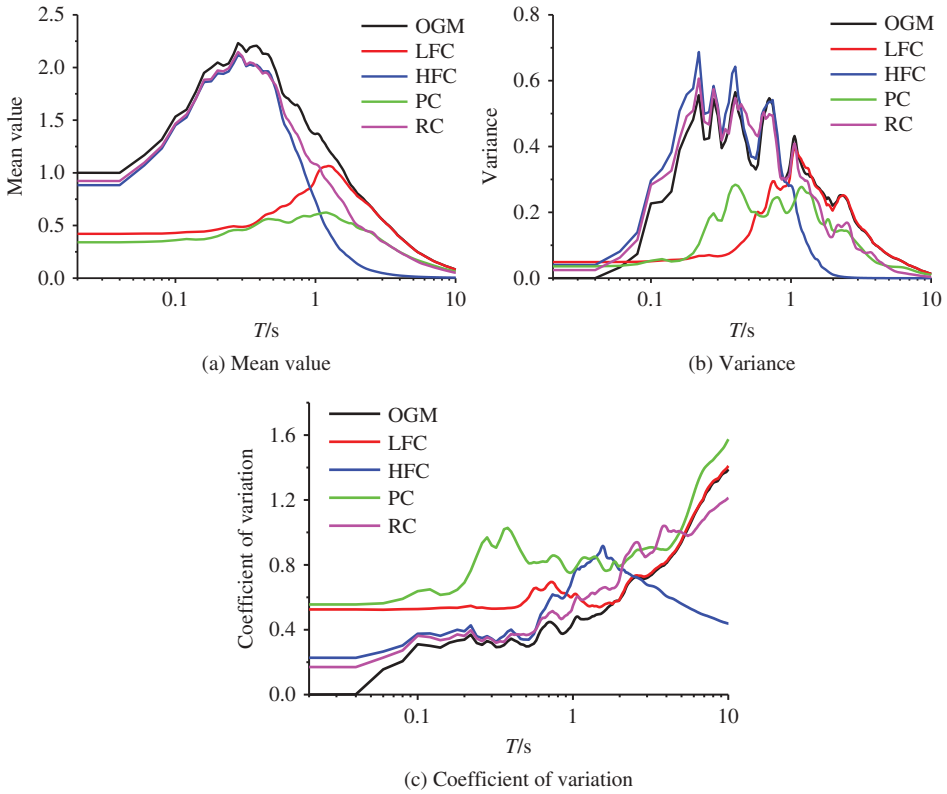

FIGURE 5 Statistical parameters of the response spectra normalized with PGA_O of five sets of data (OGM, LFC, HFC, PC, and RC).

value that illustrated in Fig. 5a. So, it can be concluded that LFC and HFC are the main factors that influence the variation of the response spectrum for pulse-type record in long- and short-period range, respectively.

Figure 5c shows the coefficient of variation of the normalized response spectra. Figure 5c carries an important message that the coefficient of variation of these components is clearly greater than that of original records in short-period region. The rigidity of a single-degree-of-freedom system will be very large when the period of the system approach to zero, then the acceleration response of the system will be consistent with the excitation. Because of the ordinates of the response spectra for OGM are normalized by PGA_O, so the spectral accelerations are close to 1 in short-period range. For components, the response spectral ordinates are normalized by PGA_O not PGA_C, hence its coefficient of variation is larger than OGM. So, the ordinate of the response spectrum for components should be normalized by itself peak value, i.e., PGA_C.

The statistical parameters of the response spectrum normalized by PGA_C of ground motion components are shown in Fig. 6. As shown in Fig. 6a, the mean values are close to 1 when periods approach to zero. In Figs. 6b –6c, both variance and coefficient of variation are close to zero when periods approach to zero. As shown in Figs. 6b–c, the values of PC are the largest in long-period region. It is consistent with previous studies which indicated that the velocity pulses included in original records show a large diversity. Even filtering the velocity pulse, the coefficient of variation of RC is still very large in long-period region.

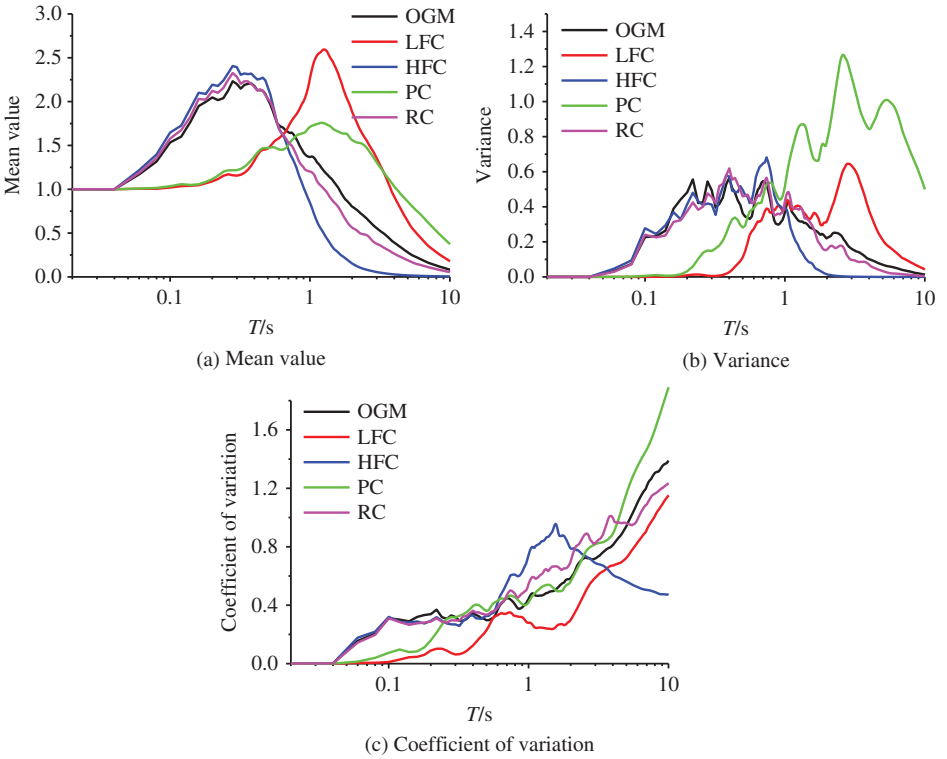

FIGURE 6 Statistical parameters of the response spectra normalized with PGA_O of original records and those of the response spectra normalized with PGA_C of four sets of ground motion components (LFC, HFC, PC, and RC).

Figure 7 illustrates the large diversity of the normalized response spectra for these five sets of data. An important observation from the figure is the existence of more than one clear acceleration peak in the acceleration response spectra for OGM, LFC, HFC, and RC. But for PC, most of their response spectra only have one clear peak. As will be discussed later, identifying the predominant peak is the key to estimating the predominant period of a record in the process of calculating bi-normalized response spectrum.

4.2. Statistical Characterizations of Bi-normalized Response Spectra

As mentioned in Sec. 1, bi-normalized response spectrum is obtained by dividing the response spectrum ordinates by the corresponding peak ground motion and by normalizing the period axis with the predominant period T_p. In this study, the predominant period T_p is defined as the period associated with the peak value of the absolute acceleration response spectrum for corresponding excitation (original record or ground motion component). The response spectrum ordinates of original records are divided by PGA_O and those of ground motion components are normalized with PGA_C.

Figure 8 shows the statistical parameters of the bi-normalized response spectra. In Fig. 8a, the differences between the peak values of the bi-normalized response spectra for those five sets of data are negligible. So it can be assumed that the maximum dynamic amplification factors of single-degree-of-freedom system when subjected to original records and to ground motion components are roughly equal to each other. In Fig. 8b,

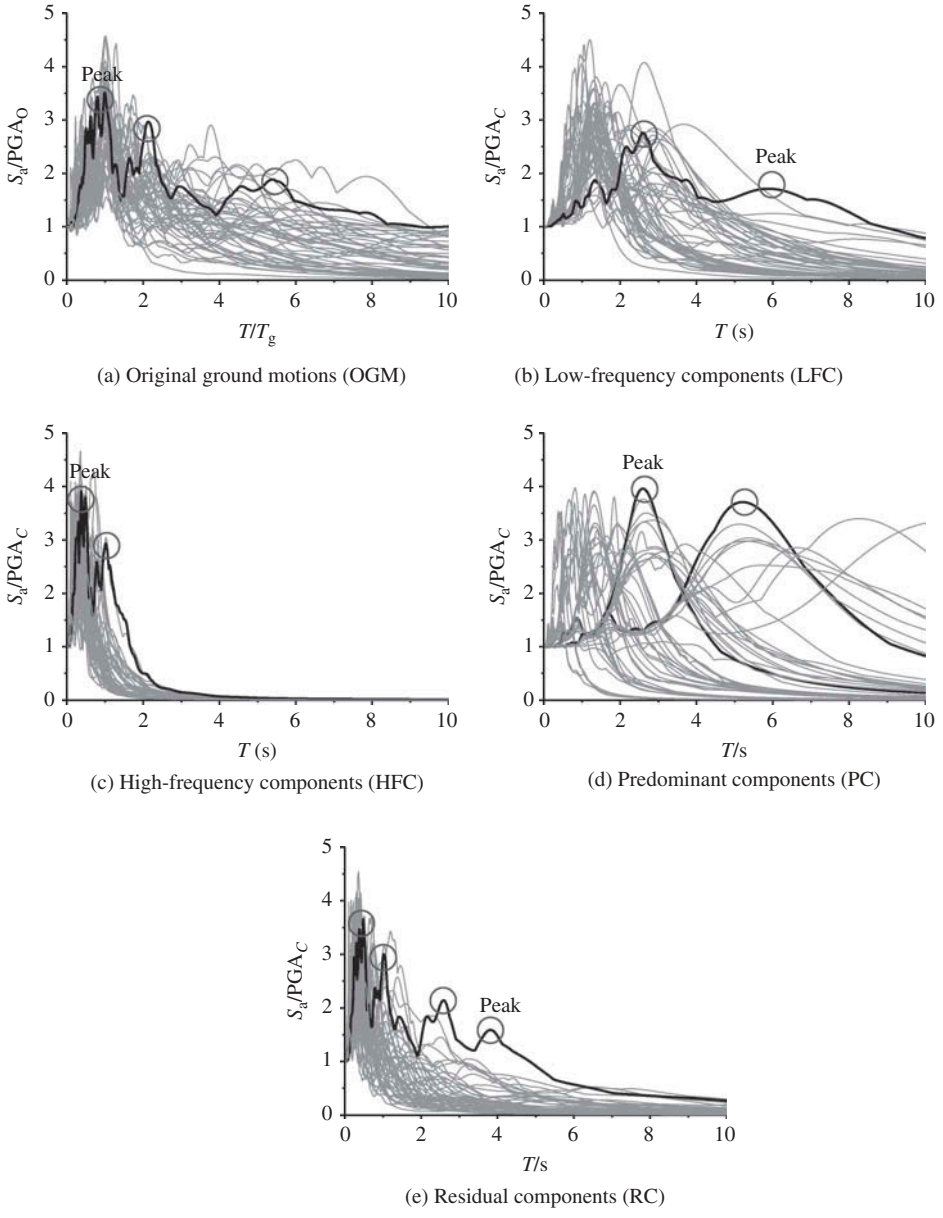

FIGURE 7 Normalized response spectra of original records (S_a/ PGA_O) and those of ground motion component (S_a/ PGA_C).

the variances of PC are the lowest, which is contrary to the results illustrated in Fig. 6b. So the bi-normalized response spectrum is more preferable for the excitations with simple frequency contents. In Fig. 8c, the coefficient of variations of HFC are the largest, so the bi-normalized response spectrum is not suitable for the excitations dominated by high-frequency contents.

Comparing with preceding Sec. 4.1, it can be seen that: (1) for PC, the statistical parameters of its bi-normalized response spectra are more preferable; (2) for OGM, LFC,

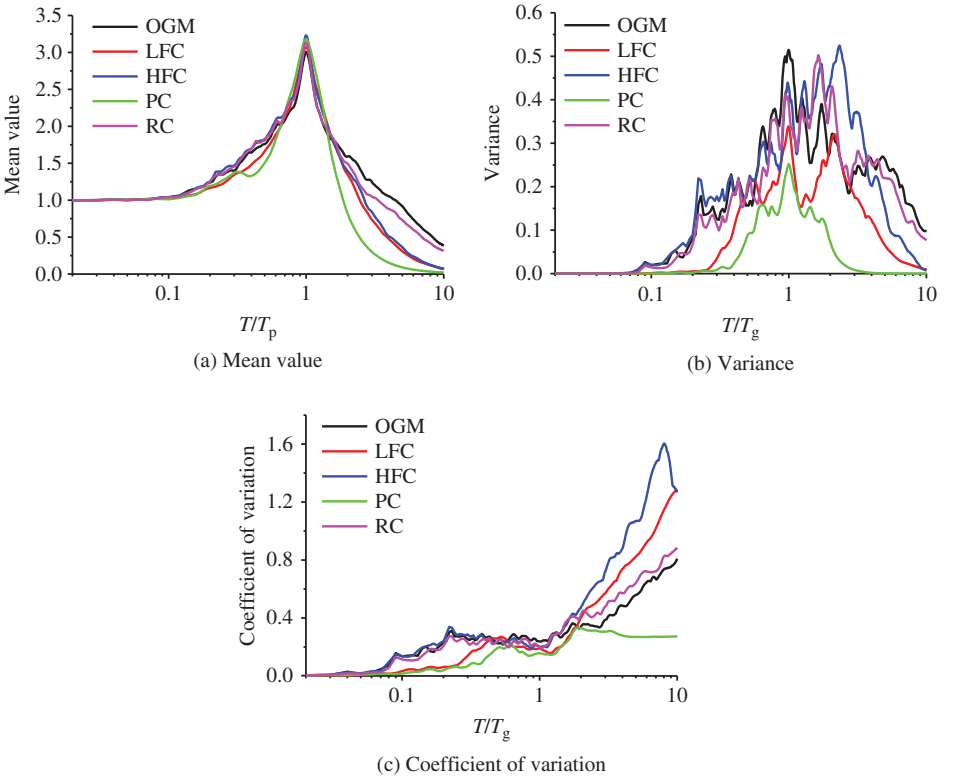

FIGURE 8 Statistical parameters of the bi-normalized response spectra of five sets of data (OGM, LFC, HFC, PC, and RC).

HFC, and RC, there are no obvious changes between the statistical parameters of their normalized response spectra and those of their bi-normalized response spectra.

4.3. Bi-normalized Response Spectra of Simple Component

As mentioned previously, for OGM, LFC, HFC, and RC, there are more than one clear peak in their acceleration response spectra. But for PC, most of their response spectra only have one clear peak. In fact, PC is one special kind of simple component. Analyses indicate that the statistical characterizations of the bi-normalized response spectra of other simple components behave the same feature with those of PC. This section comprehensively investigates the bi-normalized response spectra characteristics of SC. And the methodology for deriving design spectra which will be introduced in section 6 is mainly based on the bi-normalized response spectra of SC.

Figure 9 shows the bi-normalized response spectra of the 466 simple components mentioned above.Generally, the spectral curves are similar with each other and most of them have one clear peak. The statistical parameters of the bi-normalized response spectra of those simple components are shown in Fig. 10. It can be seen that the variance and the coefficient of variation increase gradually with the increase of damping ratio (ξ). The variance shows a peak at $T/T_g = 1$, but the coefficient of variation is not very large at the same point. The maximum coefficient of variation is about 0.5 at $\xi = 5\%$. Combining with Sec. 4.2, it can be seen that the statistical characterizations of the bi-normalized response spectra

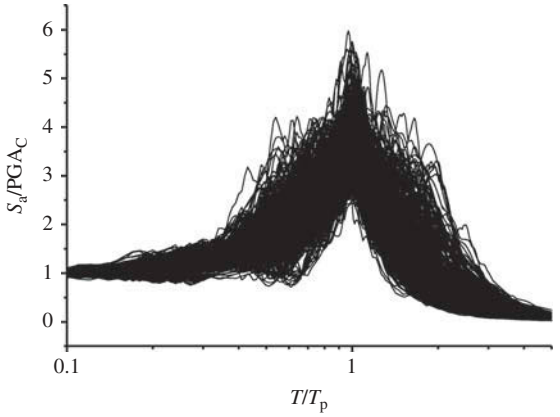

FIGURE 9 Bi-normalized response spectra of simple components.

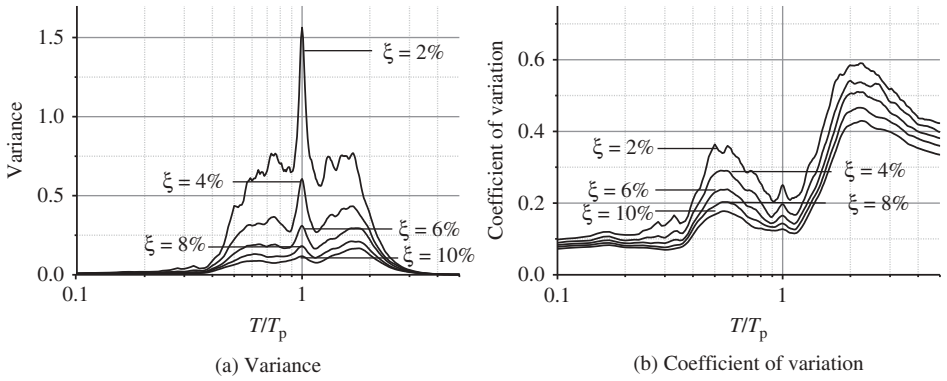

FIGURE 10 Statistical parameters of the bi-normalized response spectra of simple components.

of simple components are much better than those of original records and combination components.

The function, given in Eq. (12), which is similar with the function of the dynamic amplification factor of single-degree-of-freedom system when subjected to harmonic load, is adopted to represent the bi-normalized response spectra for SC. First, the mean bi-normalized response spectra with the damping ratio ξ range of 0–10% in the interval of 1% for the 466 simple components are computed. Then, a random effects model based on the algorithm proposed by Abrahamson and Youngs [1992] was used to conduct the regression analysis on Eq. (12):

$$\beta_{ij} = 1/\sqrt{(1 - ar_T{}^c)^2 + br_T{}^c} + \eta_i + \varepsilon_{ij}, \tag{12}$$

where $a = k_1\xi + k_2$; $b = k_3\xi + k_4$; $c = k_5(10\xi + k_6)^2 + k_7$; β_{ij} is the β (β=S_a/PGA) of the jth r_T ($r_T = T/T_g$) from the ith damping ratio ξ. $k_1 \sim k_7$ are regression parameters; η_i and ε_{ij} represent the inter- and intra-event variations, respectively, obtained using the random effects model. The inter-event and the intra-event error terms are assumed to be independent

TABLE 2 Parameters from the regression analyses for bi-normalized response spectra (Eq. (12))

Parameters	k_1	k_2	k_3	k_4	k_5	k_6	k_7	σ	τ	σ_{total}
Regression results	−0.910	−0.974	1.081	0.023	−0.308	−1.021	1.303	0.691	0.113	0.700

normally distributed random variables with variances τ^2 and σ^2, respectively. The standard error associated with the estimate of β is $\sigma_{total}^2 = \tau^2 + \sigma^2$. Results of the regression analyses for β are given in Table 2.

A comparison of the mean prediction with the averaged spectra at five damping ratio ξ levels is illustrated in Fig. 11. It is worth noting that simple component is not ideal simple harmonic wave, so the frequency contents of simple component are a little more complex than those of simple harmonic wave. And this might be the major reason that results in the phenomena that the increase rate and decrease rate of the fitted spectra are larger than those of the averaged spectra in short- and long-period region, respectively. But, the fitted spectra could generally reflect the major feature of the averaged spectra.

Figure 12 shows the absolute acceleration spectrum of an original record of TCU103 station during Chi-Chi earthquake and those of its three simple components. It can be seen that the peak value of the spectrum of simple component is close to the spectral value of the original ground motion at the predominant period T_p of simple component, but a non-ignorable difference is also existed. Considering this phenomenon, spectrum ratio that defined as $R_S = S_{\mathrm{a\,O}}|_{T=T_\mathrm{p}}/S_{\mathrm{a\,C}}|_{T=T_\mathrm{p}}$ is introduced in this article. Where $S_{\mathrm{a\,O}}$ is the absolute acceleration spectrum of original record, $S_{\mathrm{a\,C}}$ is the absolute acceleration spectrum of simple component; T_p is the predominant period of simple component. Figure 13 shows the R_S of the 466 simple components. As seen, R_S mainly distributes in the range of 1–2 except in short-period range ($T_\mathrm{p} < 0.1$s). In this article, Eq. (13) is adopted as the prediction of function express of R_S with the predominant period T_p of simple component:

$$R_\mathrm{S} = 0.136^{(\ln(T_\mathrm{p})+2.661)} + 1.347. \tag{13}$$

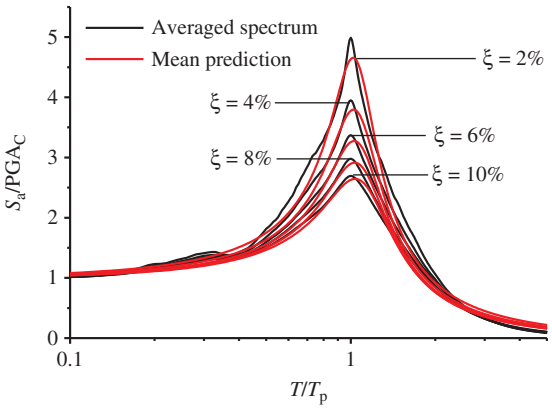

FIGURE 11 Comparison of the averaged spectra with the fitted spectra at different damping ratio levels.

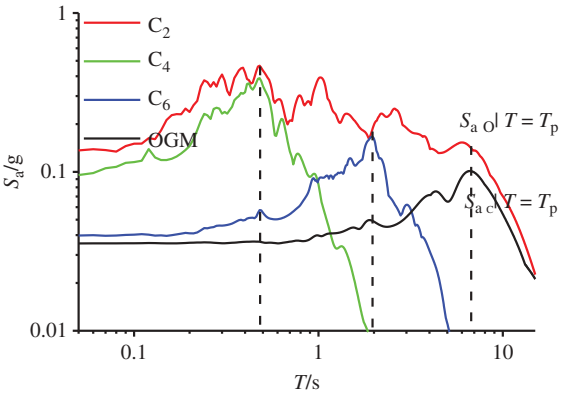

FIGURE 12 Comparison of the acceleration response spectra of an original record of TCU103 station during Chi-Chi earthquake with those of its three simple components.

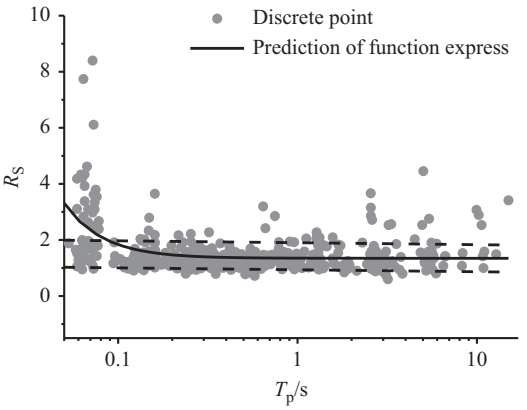

FIGURE 13 Prediction function express of R_S with the predominant period T_p of simple component.

5. Acceleration Amplitude Characterizations of Simple Components

5.1. Probability Distribution of the Acceleration Amplitude of Simple Components

This article presents probabilistic methods to evaluate the acceleration amplitude of simple components. A significant difference of the acceleration amplitude for various recordings is existed, due to the influences caused by focal mechanism, travel path and soil condition etc. In order to eliminate the influence of original records, relative acceleration amplitude, which is defined as the ratio between the amplitude of ground motion component and that of original record, $r_{PGA} = PGA_C/PGA_O$, is introduced to investigate the amplitudes of simple components in this study.

The relative acceleration amplitude r_{PGA} of the 466 simple components are shown in Fig. 14. Two samples, sample 1 with period range of 0.2–0.3 s, sample 2 with period range of 1–2 s, are selected to represent the characterization of high- and low-frequency components, respectively. Because of more components are in short-period region, so different interval lengths are selected. The number of the points in the two samples is roughly equal with each other, about 60.

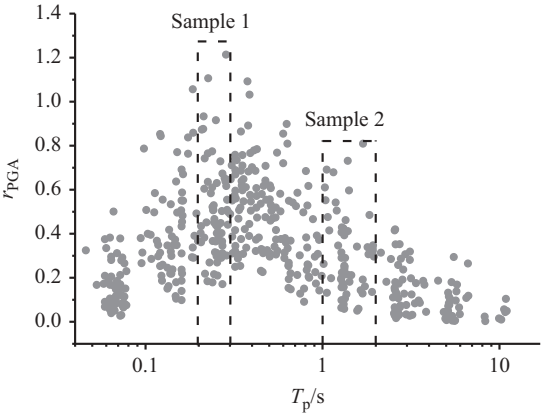

FIGURE 14 Distribution of the relative acceleration amplitude r_{PGA} with predominant period T_p.

The lognormal probability density function (given in Eq. (14)) of the relative acceleration amplitude r_{PGA} compares with the normalized relative frequencies histogram of the dataset for these two samples in Fig. 15. The Q-Q plot in Fig. 16 confirms the fact that the lognormal distribution is adequate for modeling the probability distribution of the relative acceleration amplitude r_{PGA}. This observation is consistent for all the simple components that obtained in this study. The following studies are based on the assumption that the distribution of r_{PGA} obeys lognormal distribution in a given period point:

$$f(x) = \frac{1}{\sigma r_{PGA}\sqrt{2\pi}} \exp[-\frac{1}{2}(\frac{\ln r_{PGA} - \mu}{\sigma})^2]. \tag{14}$$

5.2. Method for Determining the Probability Model

As mentioned above, the lognormal distribution is adequate for modeling the probability distribution of the relative acceleration amplitude r_{PGA}. Due to the data deficiency especially in long-period region, the parameters, μ and σ, cannot be precisely obtained

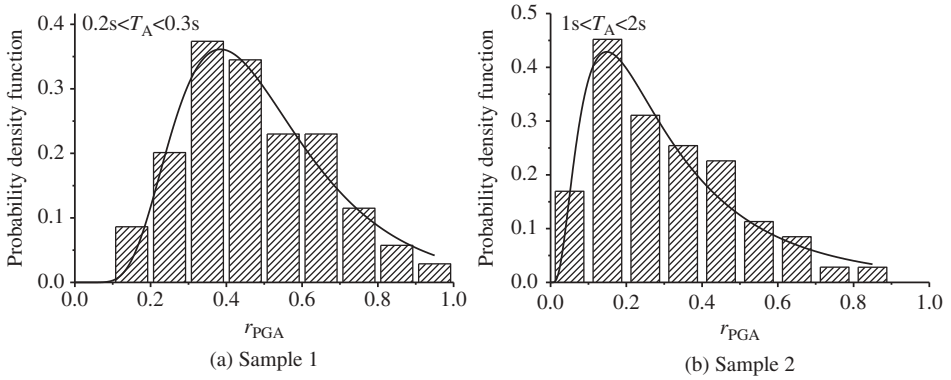

FIGURE 15 Probability density function of r_{PGA} vs. normalized relative frequencies histogram.

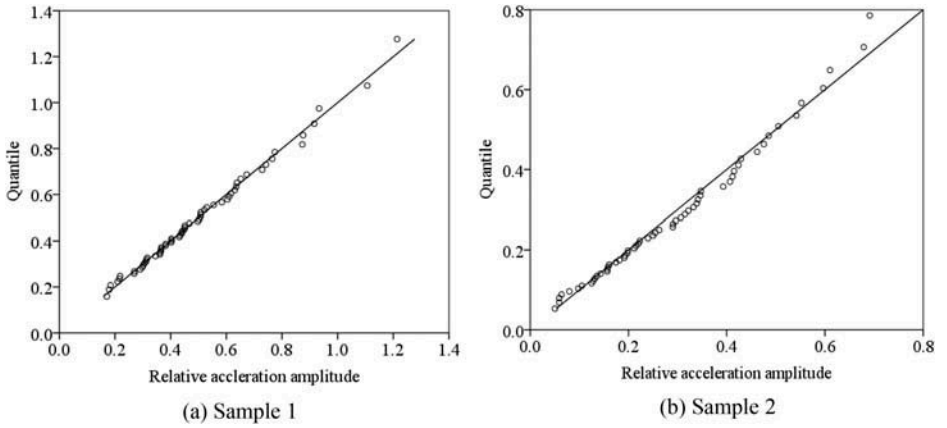

FIGURE 16 Q-Q plot for values of relative acceleration amplitude r_{PGA}.

through regression analysis. In lognormal distribution, the mean and the median can be calculated by Eqs. (15) and (16), respectively:

$$r_{\mathrm{PGA\ mean}} = e^{u+\sigma^2/2} \tag{15}$$

$$r_{\mathrm{PGA\ median}} = e^{u} \tag{16}$$

So μ and σ can be obtained by Eqs. (17)–(18). In this study, the two parameters, μ and σ, are obtained through the relationship between the mean and the median:

$$\mu = \ln(r_{\mathrm{PGA\ median}}) \tag{17}$$

$$\sigma = \sqrt{2(\ln(r_{\mathrm{PGA\ mean}}) - \ln(r_{\mathrm{PGA\ median}}))}. \tag{18}$$

For acquiring more precise statistical results of the mean and the median, ten period intervals are divided. Figures 17a–b show the statistical values and the regression results for

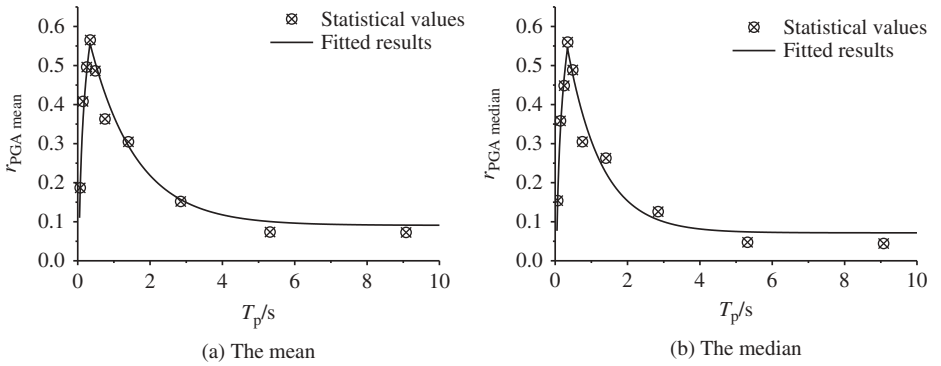

FIGURE 17 Regression results of the mean and of the median of the relative acceleration amplitude r_{PGA}.

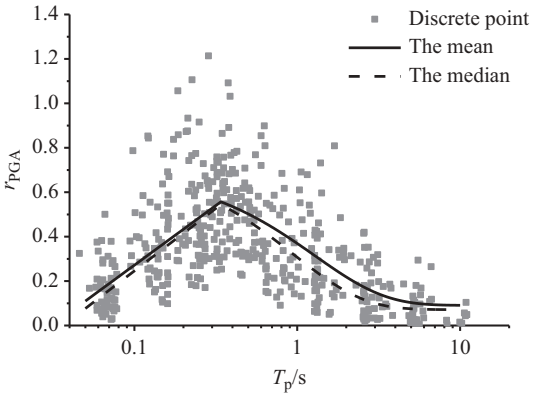

FIGURE 18 Regression results of the mean and the median.

the mean and the median respectively. The final regression results are given in Eqs. (19)–(20). The comparison between the regression results of the mean and the median is shown in Fig. 18:

$$r_{\text{PGA mean}} = \begin{cases} 0.233\ln(T_p) + 0.808 & 0 < T_p < 0.34 \\ 0.459^{(T_p+0.639)} + 0.091 & 0.34 \le T_p \le 10 \end{cases} \tag{19}$$

$$r_{\text{PGA median}} = \begin{cases} 0.244\ln(T_p) + 0.808 & 0 < T_p < 0.34 \\ 0.347^{(T_p+0.367)} + 0.072 & 0.34 \le T_p \le 10. \end{cases} \tag{20}$$

Through the analyses mentioned above, μ and σ can be easily determined. Then the probability distribution function of r_{PGA} can be defined in a given period point. The probability density and the probability distribution functions at five period points, 0.5 s, 1 s, 2 s, 4 s, and 8 s are illustrated in Figs. 19a–b, respectively. It can be seen that the probability density functions behave the shape of "short and wide" in short-period region, and behave the shape of "tall and narrow" in long-period region. In an given probability P where P($r_{PGA} < r_{PGA\,P}$) = P, the $r_{PGA\,P}$ in long-period region will be less than that in short-period region. The r_{PGA} with six probability levels, 10%, 30%, 50%, 70%, 80%, and 90% are shown in Fig. 20. The methodology for determining r_{PGA} will be used for deriving design spectrum in Sec. 6.

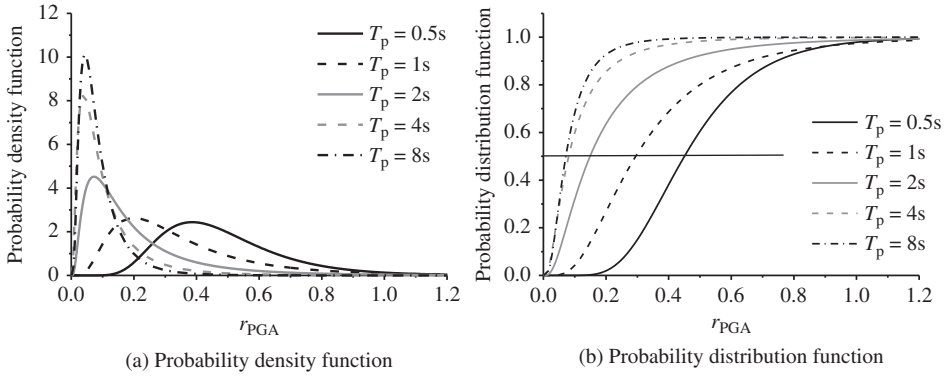

(a) Probability density function (b) Probability distribution function

FIGURE 19 Probability density function and probability distribution function of r_{PGA} at five period points, 0.5 s, 1 s, 2 s, 4 s, and 8 s.

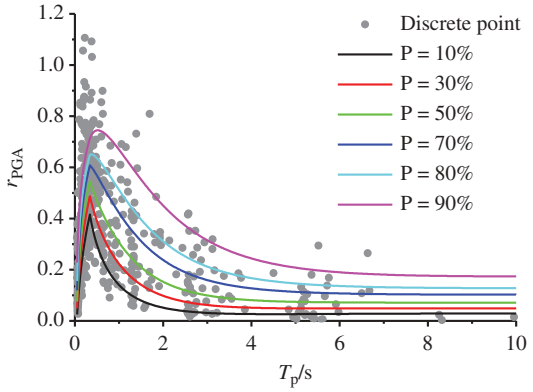

FIGURE 20 Relative acceleration amplitude r_{PGA} at six levels of probability.

6. Methodology for Deriving Design Acceleration Spectrum

6.1. Near-Fault Response Spectrum (NFRS)

If a single-degree-of-freedom system with the natural vibration period of T_S is subjected to a simple component with the predominant period of T_p, the maximum acceleration response of the system can be computed by Eq. (21):

$$s_{a\,C} = \mathrm{PGA_O} \cdot r_{PGA} \cdot \beta, \tag{21}$$

where $s_{a\,C}$ is the maximum acceleration response of single-degree-of-freedom system to ground motion component; r_{PGA} can be obtained by probabilistic method which is mentioned in section 5; β is the dynamic amplification factor and is defined by Eq. (12); $\mathrm{PGA_O}$ is the peak ground motion of the corresponding original record. As shown in Fig. 21, with the increase of the closest distance to rupture R, $\mathrm{PGA_O}$ decreases gradually. The prediction relationship of $\mathrm{PGA_O}$ with R is given in Eq. (22), and the mean of $\mathrm{PGA_O}$ for the 53 pulse-type records is about 0.5 g:

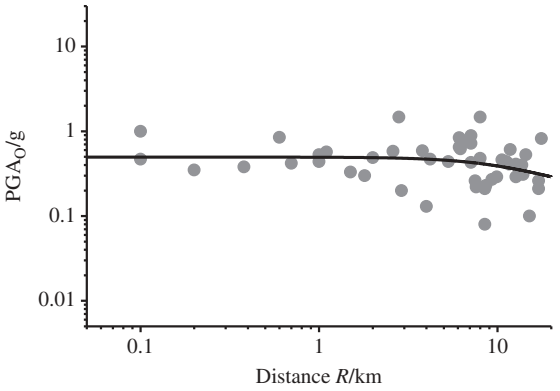

FIGURE 21 Attenuation relationship of $\mathrm{PGA_O}$ with the closest distance to rupture R.

$$\log_{10}(\mathrm{PGA_O}) = -0.3\log_{10}(R^2 + 9^2) + 0.268. \tag{22}$$

Figure 22 shows the $s_{a\,C}$ of a single-degree-of-freedom system with the period of 4.0 s at three probabilistic levels of $r_{\mathrm{PGA\,P}}$, 30%, 50%, and 80%. Figure 22 reflects the response variation of single-degree-of-freedom system to a series of simple components at different probabilistic. So the influence caused by simple components on single-degree-of-freedom system can be evaluated through this method. In this study the function defined by Eq. (22) is named as Components Influence Spectrum (CIF).

As shown in Fig. 12, the response of a single-degree-of-freedom system subjected to simple components is less than that to original records. If an original record includes a simple component with the predominant period of T_p, and the maximum acceleration response of a single-degree-of-freedom system with the natural vibration period $T_s = T_p$ to the simple component is $s_{a\,C}$, then the maximum acceleration response of the system to the original record can be predicted by Eq. (23):

$$s_{a\,O} = s_{a\,C} \cdot R_s, \tag{23}$$

where $s_{a\,O}$ is the maximum acceleration response of a single-degree-of-freedom system to original record; R_S is spectrum ratio which is defined by Eq. (13). Figure 23 shows the $s_{a\,O}$ of a single-degree-of-freedom system with the period of 4.0 s:

$$S_{a\,C} = \mathrm{PGA_O} \cdot r_{\mathrm{PGA}} \cdot \beta_{\max} \tag{24}$$

$$S_{a\,O} = \mathrm{PGA_O} \cdot r_{\mathrm{PGA}} \cdot \beta_{\max} \cdot R_s. \tag{25}$$

Equations (24) and (25) are the envelope curves of Eqs. (22) and (23), respectively. Equations (24) and (25) with the r_{PGA} of P = 50% are illustrated in Figs. 24a and 24b, respectively. As seen, the values of Eq. (25) can be increased effectively especially in short-period region through considering R_S. Equation (25) is the function of the maximum acceleration response of single-degree-of-freedom system to a ground motion with the period of the system, having the same concept with that of design spectrum. In this article, Eq. (25) is adopted to consider the effects of pulse-type records in seismic design, and named as Near-Fault Response Spectrum (NFRS).

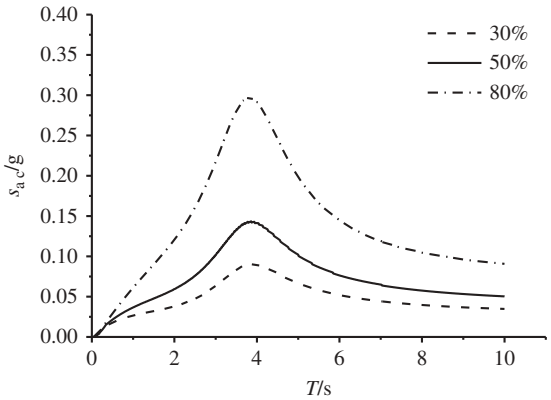

FIGURE 22 Components Influence Spectra of a single-degree-of-freedom system with the vibration period of 4 s.

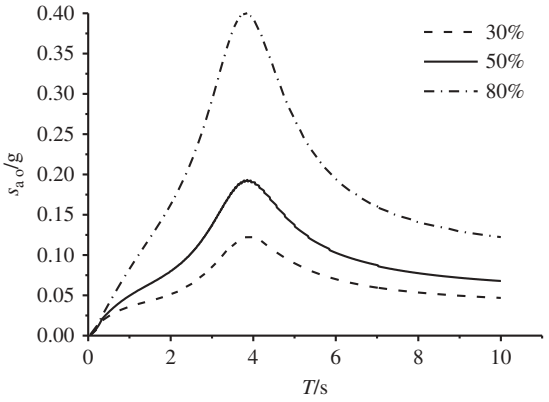

FIGURE 23 $s_{a\,O}$ of a single-degree-of-freedom system with the vibration period of 4 s.

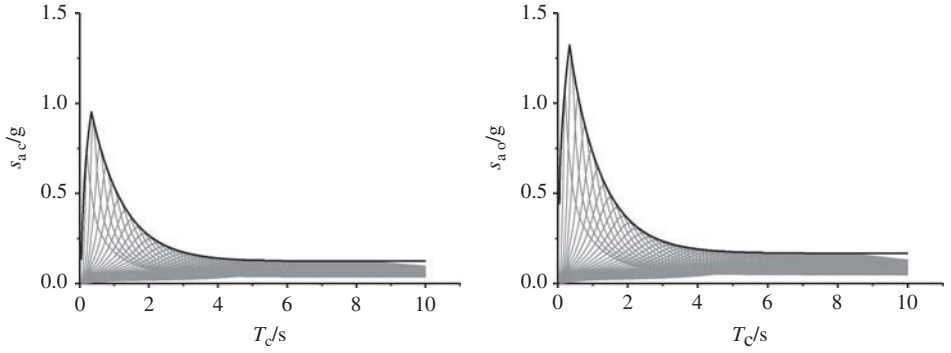

(a) Envelope curves of s_a C

(b) Envelope curves of s_a O

FIGURE 24 Envelope curves ($S_{a\,C}$, $S_{a\,O}$ defined in Eqs. (24) and (25)) of $s_{a\,C}$, $s_{a\,O}$ that defined in Eqs. (21) and (23).

6.2. Comparison of NFRS with the Design Spectra for Chinese, European, and American Codes

Figure 25 compares the Near-Fault Response Spectrum (NFRS) together with the design spectra for Chinese code (GB50011-2010), European code (Eurocode 8), and American code (UBC97, IBC 2012). It can be seen that: (1) in short-period region, Chinese design spectrum is the lowest, but it gradually over than others because of the linear decreasing in long-period region; (2) in short-period region, Eurocode 8 design spectrum is the largest, but in long-period region, it gradually decreases and becomes the lowest; (3) UBC97 design spectrum is similar with Chinese design spectrum when does not consider the near field effect; (4) UBC97 design spectrum is close to the averaged spectrum when considers the near field effect. The averaged spectrum, gray solid line in Fig. 25, is obtained by averaging the normalized spectra of the 53 pulse-type records and then multiplying the mean of the PGA_O, 0.5 g. Therefore, UBC97 design spectrum, to an extent, can reflect the averaged spectrum characterizations of pulse-type records through incorporating near-source factors.

In IBC 2012, there is no clear definition of how to consider near source effects. In order to compare with the averaged spectrum, the design parameters S_{DS} and S_{D1} are assumed

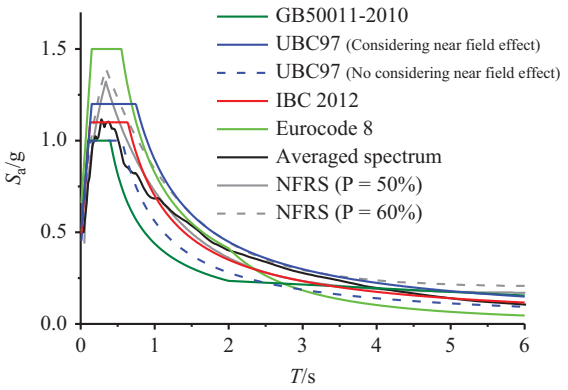

FIGURE 25 Comparison of the near-fault spectra obtained in this study with the design spectra for Chinese, European, and American code. *Note*: (1) In GB50011-2010, the design parameters ($\alpha_{max} = 1.0$ g, $T_g = 0.4$ s) are selected in accordance with VIII zone under rare occurrence earthquake, in consideration of the 53 pulse-type records are selected from large magnitude earthquakes. (2) In UBC97, the design parameters ($N_a = 1.2$; $N_v = 1.6$, $T_s = C_v/2.5C_a$, $T_o = 0.2T_s$) are selected in accordance with S_C soil profile type, Zone 4, "A" seismic source type, "5 km" closest distance. (3) In IBC 2012, the design parameters ($S_{DS} = 1.1$ g, $S_{D1} = 0.7$ g) are selected. In this case, the design peak spectral acceleration is equal to the peak value of averaged spectrum, and the design spectral acceleration is equal to the averaged spectrum in $T = 1.0$ s. (4) In Eurocode 8, the ground type is applied to B with V_{s30} (m/s) range of 360–800, then the design parameters: $a_g = 0.5$ g, $S = 1.0$, $T_B = 0.15$ s, $T_C = 0.55$ s, and $T_D = 2.0$ s. In addition, Eurocode 8 notes that the spectrum should normally be applied for vibration periods not exceeding 4.0 s. For structures with vibration periods longer than 4.0 s, a more complete definition of the elastic displacement spectrum is possible. But in order to compare with these codes, the vibration periods are lengthened to 6 s.

as 1.1 g and 0.7 g, respectively. In this case, the design peak spectral acceleration is equal to the peak value of averaged spectrum, and the design spectral acceleration is equal to the averaged spectrum in $T = 1.0$ s. It can be seen that even the IBC 2012 design spectrum could roughly reflect the characteristic of the averaged spectrum but its spectral values are visibly less than those of the averaged spectrum in long period region ($T > 1.0$ s). Therefore, there still exist some deficiencies in IBC 2012, in consideration of the decay model in long period region of IBC 2012 design spectrum cannot commendably reflect the response spectral characteristic for pulse-type ground motions.

In Fig. 25, the UBC97 design spectrum when considering the near field effect with the closest distance of 5km is similar with the NFRS with the probability of 60%. But it is still lower than many of the response spectra of the 53 pulse-type records, as shown in Fig. 26. The values of UBC97 design spectrum can be increased by decreasing the closest distance. In Fig. 26, the UBC97 design spectral values with the closest distance less than 2 km increase significantly in short-period region, but change little in long-period region. As mentioned above, Near-Fault Response Spectrum (NFRS) can be effectively modified by adjusting the probability of r_{PGA}. As shown in Fig. 25, the NFRS with probability of 90% can be almost used as the envelope curve of the response spectra for the 53 pulse-type records. In short-period region ($T < 0.5$ s), the NFRS with probability of 80% is close to the UBC97 design spectrum with the closest distance less than 2 km. But in long-period

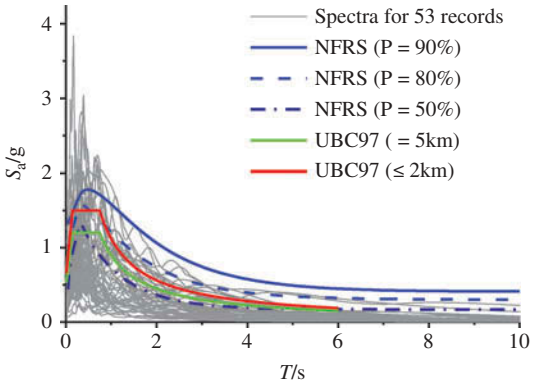

FIGURE 26 Comparison of the near-fault spectra obtained in this study with UBC97 design spectra.

region, the spectral shape of NFRS is more in line with the characterizations of the response spectra of pulse-type ground motions.

6.3. Advantages and Disadvantages of the Methodology Proposed in this Study

In order to quantify the special effects of forward-directivity and to develop appropriate design spectra in the near-fault region, Mavroeidis [2004] attempted to capture the salient characteristics of pulse-type ground motions and develop new approaches to build design spectral models. Xu *et al.* [2006] proposed method to correlate simple pulses to available parameters relationships in constructing design spectra for pulse-type ground motions. These research works have provided insight on primary aspects of near-fault motions and desirable criterion on structural seismic design. However, these approaches for prediction of near-fault design spectra were mainly based on simple mathematical pulse models. The characterizations of real pulse-type ground motions might be more preferable in engineering applications. This article provided a new methodology for investigating ground motion characteristics and for deriving design spectrum through decomposed method. The components obtained by decomposed method are real contents of corresponding original motion. And more detailed and real characterizations of pulse-type ground motions can be revealed through this method.

In traditional method, most of the design spectra are obtained by averaging a number of response spectra of various ground motion records. Xu *et al.* [2007] computed the pseudo-velocity response spectra, the corresponding normalized and bi-normalized spectra for the same set of pulse-type strong motions, and then design spectra are constructed. In this way, the final spectral shape may change little even though the parameters, such as amplitude, period, etc., change greatly. So for traditional method, the statistical property, which is always represented by dispersion, is not consistently satisfied in engineering application. The methodology proposed in this study is based on ground motion components instead of original records. Even the frequencies and amplitudes are different greatly for different simple component, but the bi-normalized response spectral shapes of different simple components are mostly similar with each other. And the spectral values can be modified through probabilistic method. As a result, the final shapes of the spectra with different probabilities are not fixed, and are more in line with the characterizations of the response spectra of pulse-type ground motions.

At present, not ground motion components but original ground motion records are employed in the field of structure seismic design. So it will be the major problem of the methodology introduced in this study. Actually, the influences of some contents on an elastic single-degree-of-freedom system are negligible when the vibration frequencies of these contents are far from the vibration frequency of the system. And these contents, to an extent, can be considered as a special noise. Hence, the methodology proposed in this study is adequate for representing the characteristics of elastic response spectra. This article merely provides a preliminary exploration that investigating ground motion characteristic through ground motion components not original ground motion, so there still need further investigation and discussion.

7. Conclusions

This article analyzed the characterizations of pulse-type records through ground motion components instead of original records. The analytical study performed in this paper has led to the following preliminary conclusions.

1. Frequency content is one of the critical factors that result in the large diversity of the response spectra of pulse-type ground motions. The influence caused by frequency content on response spectrum can be quantitatively analyzed through ground motion components obtained by multi-resolution decomposed method.
2. Simple component obtained by multi-resolution decomposed method behaves preferable statistical characterizations than original record. The coefficient of variation of the bi-normalized response spectra for simple component is significantly lower than that for original record.
3. The lognormal distribution is adequate for modeling the probability distribution of the relative acceleration amplitude (r_{PGA}) of simple component. Due to the data deficiency, the probabilistic model of r_{PGA} was established through the relationship of μ and σ with the mean and the median.
4. A methodology, named as Near-Fault Response Spectrum (NFRS), which could incorporate the special effects caused by pulse-type records, was proposed based on the analysis results of simple components. The comparison of the methodology with the design spectra of several countries codes indicates that NFRS might be a reliable candidate for the code-based design spectrum especially for structures constructed close to active fault.

Admittedly, there are still a lot of problems to be solved before the application of this methodology in engineering field. The influence caused by some factors such as source mechanism, magnitude, soil condition, epicentral distance etc., on frequency content is one of the most urgent problems. The methodology will be gradually improved in the further study, and will be tested whether it is suitable for other types of ground motions. The growing application of displacement-based design in earthquake engineering urges for a reliable determination of the displacement demand. The methodology for developing acceleration spectrum proposed in this article might provide an alternative way to determine the displacement spectrum, and it will be investigated in the further study.

Funding

The research was supported by The Major Research Plan of National Natural Science Foundation of China (91215301), the National Natural Science Foundation of China (51178152, 51238012), Project Supported by Natural Scientific Research Innovation

Foundation in Harbin Institute of Technology (HIT.NSRIF.2011115, HIT.KISTP.2014033), and Co-operative Innovation Center of Engineering Construction and Safety in Shandong Peninsula Blue Economic Zone, these are gratefully acknowledged.

References

Abrahamson, N. A. and Youngs, R. R. [1992] "A stable algorithm for regression analyses using," *Bulletin of the Seismological Society of America* **82**(1), 505–510.

Adanur, S., Altunisik, A. C., Bayraktar, A., and Akköse, M. [2012] "Comparison of near-fault and far-fault ground motion effects on geometrically nonlinear earthquake behavior of suspension bridges," *Natural Hazards* **64**(1), 593–614.

Akkar, S., Yazgan, U., and Gülkan P. [2005] "Drift estimates in frame buildings subjected to near-fault ground motions," *Journal of Structural Engineering* **131**(7), 1014–1024.

Alavi, B. and Krawinkler, H. [2000] "Consideration of near-fault ground motion effects in seismic design," *Proc. of the 12th World Conference on Earthquake Engineering*, New Zealand, pp. 1–8.

Baker, J. W. [2007] "Quantitative classification of near-fault ground motions using wavelet analysis," *Bulletin of Seismological Society of America* **97**(5), 1486–1501.

Bommer, J. J. and Martínez-Pereira, A. [1999] "The effective duration of earthquake strong motion," *Journal of Earthquake Engineering* **3**(2), 127–72.

Bommer, J. J., Magenes, G., Hancock, J., and Penazzo, P. [2004] "The influence of strong-motion duration on the seismic response of masonry structures," *Bulletin Earthquake Engneering* **2**(1), 1–26.

Bray, J. D. and Rodriguez-Marek, A. [2004] "Characterization of forward-directivity ground motions in the near-fault region," *Soil Dynamics and Earthquake Engineering* **24**(11), 815–828.

Galal, K. and Ghobarah, A. [2006] "Effect of near-fault earthquakes on North American," *Nuclear Engineering and Design* **236**(18), 1928–1936.

Gazetas, G. [2012] "Some presumptions on the nature of base excitation may erroneously affect the response of strongly inelastic systems," *Proc. of the 15th World Conference on Earthquake Engineering*, Lisbon, Portugal.

Ghahari, S. F., Jahankhah, H., and Ghannad, M. A. [2010] "Study on elastic response of structures to near-fault ground motions through record decomposition," *Soil Dynamics and Earthquake Engineering* **30**(7), 53–546.

Hall, J. F., Heaton, T. H., Halling, M. W., and Wald, J. D. [1995] "Near source ground motion and its effects on flexible buildings," *Earthquake Spectra* **11**(4), 569–605.

Hancock, J. and Bommer, J. J. [2007] "Using spectral matched records to explore the influence of strong-motion duration on inelastic structural response," *Soil Dynamics and Earthquake Engineering* **27**(4), 291–299.

Hubbard, D. T. and Mavroeidis, G. P. [2011] "Damping coefficients for near-fault ground motion response spectra," *Soil Dynamics and Earthquake Engineering* **31**(3), 401–417

Krawinkler, H. and Alavi, B. "Development of an improved design procedure for near-fault ground motions," *SMIP 98 seminar on utilization of strong motion data*, Oakland, California, 1998.

Luco, N. and Cornell, C. A. [2007] "Structure-specific scalar intensity measures for near-source and ordinary earthquake ground motions," *Earthquake Spectra* **23**(2), 357–392.

Makris, N. [1997] "Rigidity–plasticity–viscosity: can electrorheological dampers protect base-isolated structures from near-source ground motions ?" *Earthquake Engineering and Structural Dynamics* **26**(5), 571–591.

Mavroeidis, G. P., Dong, G., and Papageorgiou, A. S. [2003] "A mathematical representation of near-fault ground motions," *Bulletin of the Seismological Society of America* **93**(3), 1099–1131.

Mavroeidis, G. P., Dong, G., and Papageorgiou, A. S. [2004]"Near-fault ground motions, and the response of elastic and inelastic single-degree-of-freedom (SDOF) systems," *Earthquake Engineering and Structural Dynamics* **33**(9), 1023–1049.

Maniatakis, C. A. and Spyrakos, C. C. [2012] "A new methodology to determine elastic displacement spectra in the near-fault region," *Soil Dynamics and Earthquake Engineering* **35**, 41–58.

Mallat, S. G. [1989] "A theory for multiresolution signal decomposition," *IEEE Transactions on Pattern Recognition and Machine Intelligence* **11**(7), 674–693.

Menum, C. and Fu, Q. [2002] "An analytical model for near-fault ground motions and the response of SDOF systems," *Proc. of the 7th U.S. National Conference on Earthquake Engineering*, Earthquake Engineering Research Institute, Boston, Massachusetts.

Montejo, L. A. and Kowalsky, M. J. [2008] "Estimation of frequency-dependent strong motion duration via wavelets and its influence on nonlinear seismic response," *Computer-Aided Civil and Infrastructure Engineering* **23**(4), 253–264.

Pavel, F., Vacareanu, R., and Lungu, D. [2014] "Bi-normalized response spectra for various frequency content ground motions," *Journal of Earthquake Engineering* **18**(2), 264–289.

Ruch, D. K. and Van Fleet, P. J. [2009] *Wavelet theory: An elementary approach with applications*, John Wiley & Sons,Inc., Hoboken, New Jersey.

Somerville, P. G., Smith, N. F., Graves, R. W., and Abrahamson, N. A. [1997] "Modification of empirical strong ground motion attenuation relations to include the amplitude and duration effects of rupture directivity," *Seismological Research Letters* **68**(1), 199–222.

Somerville, P. G. [2003] "Magnitude scaling of the near fault rupture directivity pulse," *Physics of the Earth and Planetary Interiors* **137**(1–4), 201–212.

Xu, L. J. and Xie, L. L. [2004] "Bi-normalized response spectral characteristics of the 1999 Chi-Chi earthquake," *Earthquake Engineering and Engineering Vibration* **3**(2), 147–155.

Xu, L. J. and Xie, L. L. [2007] "Near-fault ground motion bi-normalized pseudo-velocity spectra and its applications," *Acta Seismologica Sinica* **20**(5), 544–552.

Xu, L. J., Rodriguez-Marek, A., and Xie, L. L. [2006] "Design spectra including effect of rupture directivity in near-fault region," *Earthquake Engineering and Engineering Vibration* **5**(2), 159–170.

Yaghmaei-Sabegh, S. [2010] "Detection of pulse-like ground motions based on continues wavelet transform," *Journal of Seismology* **14**(4), 715–726.

Yaghmaei-Sabegh, S. [2012] "Application of wavelet transforms on characterization of inelastic displacement ratio spectra for pulse-like ground motions," *Journal of Earthquake Engineering* **16**(4), 561–578.

Zhao, G. C., Xu, L. J., and Xie, L. L. "On near-fault ground motion characteristics through multi-scale method," *Chinese Journal of Geophysics* **56**(12), 4153–4163.

Ziotopoulou, A. and Gazetas, G. [2010] "Are current design spectra sufficient for soil-structure systems on soft soils?" in *Advances in Performance-Based Earthquake Engineering*, ed. M. Fardis (Springer, Dordrecht) pp. 79–87.